# Phenomenological model of suspended sediment transport in a small tropical catchment

Amande Roque-Bernard[1], Antoine Lucas[1], Eric Gayer[1], Pascal Allemand[2], Céline Dessert[1], and Eric Lajeunesse[1]

[1]Université Paris Cité, Institut de physique du globe de Paris, CNRS, F-75005, Paris, France
[2]Université de Lyon, Université Lyon 1 & ENS Lyon & CNRS, Laboratoire de Géologie de Lyon, Terre Planètes Environnement, UMR 5276, 69100 Villeurbanne, France

**Correspondence:** A. Roque-Bernard (a.roqber@gmail.com), A. Lucas (lucas@ipgp.fr)

**Abstract.** We develop a phenomenological model of suspended-sediment transport on the basis of data acquired in the Capesterre river, which drains a small tropical catchment in Guadeloupe. The model correctly represents the transport of suspended sediment during floods, provided that the relation between concentration and water-level forms a counterclockwise loop. In the model, the properties of the sediment and of the river are all lumped into four parameters : a settling velocity
5  related to the size of the suspended sediment, a threshold water-level which acts as a proxy for the threshold shear stress, a characteristic erosion rate and a dimensionless exponent, both of which are related to the availability of fine sediment. The assimilation of field data to our model shows that the value of the parameters change from one flood to the next, probably reflecting changes in the characteristics of the river and the sediment. Finally, a test of the model against data acquired in a small catchment in the french Alps, suggests that the model is versatile enough to be used in diverse hydrological settings.

10  ## 1 Introduction

Rivers transport sediments according to their size. Coarse particles, like gravels or pebbles, bounce and roll above the sediment bed (Bagnold, 1973). Finer sediments, like silt, clay or even sand behave differently: their falling velocity is comparable to the fluctuations of the flow velocity induced by turbulence, and they remain suspended in the water column, trapped by turbulent eddies (Van Rijn, 1984). They thus advance with the flow, until they eventually settle back on the river bed (Phillips et al., 2019).

15  This suspended load is often the main contribution to the sediment discharge that a river carries out of its watershed (Turowski et al., 2010; Liu et al., 2011). It is therefore a major component of the erosion of continental surfaces (Summerfield and Hulton, 1994; Syvitski et al., 2003). Yet the matter suspended in a river does not entirely consists of sediment; it also includes nutrients, particulate organic matter, carbon, micro-plastics, colloidal particles, and various contaminants (e.g., D'Avignon et al., 2022). Suspended load thus affects the quality of water and riverine ecological habitats (Suttle et al., 2004; Battin et al., 2008; Lloret

20  et al., 2013a; Koiter et al., 2013).

The simplest way to estimate the suspended load carried by a river is to filter a sample of water collected in the stream, at a point where water is well mixed. The weight of the filter, once it is dried, gives a measure of the concentration of sediment, which, combined with the flow discharge, yields the rate of suspended sediment transport (Bierman and Montgomery, 2014).

In practice, however, this long and tedious procedure is inappropriate for high frequency measurements. Instead, in-situ mon-

25  itoring of the suspended load often relies on the use of a turbidimeter, an instrument capable of measuring the turbidity of the

river at a high frequency and over long periods of time (Turowski et al., 2010; Esteves et al., 2019). Turbidity measures the

amount of light scattered by the suspended particles in the water column. It is thus a convenient proxy for the suspended load

concentration. Turbidity, however, also depends on the size distribution of the suspended particles, on their shape, and on their

chemical composition. Its conversion into a sediment concentration thus requires an on-site calibration, which ultimately relies

30  on the filtering of water samples (Minella et al., 2008).

Field measurements show that the concentration of suspended sediment fluctuates with the river discharge, and culminates

during floods. Based on this observation, it is tempting to use discharge as a proxy for suspended load (e.g., Ahn and Stein-

schneider, 2018). Yet, the relation between discharge and concentration is not univocal: when observed at the scale of a single

flood event, it often exhibits a hysteretic loop (e.g., Williams, 1989). These loops are observed under various geological and

35  climatic settings, independently of the size of the catchment that the river drains (Langlois et al., 2005; Bača, 2008; Eder et al.,

2010; Ziegler et al., 2014).

Many factors combine to shape this hysteretic behavior. First of all, the suspended load concentration adjusts to the local

shear stress over a characteristic time that depends on the flow depth and the particle settling velocity (Claudin et al., 2011). The

resulting delay between discharge and sediment concentration induces a counterclockwise loop. In gravel bed rivers, fine parti-

40  cles are often trapped below a layer of coarse sediments such as pebbles, a phenomenon known as armoring (Frey and Church,

2009; Ferdowsi et al., 2017a). The river bed then acts as a sediment buffer that stores and releases fine particles according to its

own dynamics, altering the shape of the concentration-discharge relationship (Orwin and Smart, 2004; Turowski et al., 2010;

Park and Hunt, 2017; Guillon et al., 2018; Misset et al., 2019b). Fine particles, however, do not always originate from the river

bed. During storms, hillslope runoff, landsliding, and bank erosion may also feed the river with a significant quantity of fine

45  particles (Hovius et al., 2000; Allemand et al., 2014). The resulting incoming flux of external particles influences the shape of

the concentration-discharge relationship in a complex way (e.g., Asselman, 1999; Smith and Dragovich, 2009; Misset et al.,

2019a). Finally, if the velocity of the flow that carries the suspended sediment is smaller than the celerity of the flood wave,

the resulting delay between the discharge and the sediment peak induces a counterclockwise loop. This effect may dominate

the discharge-concentration relationship if the distance traveled by the suspended particles is long enough (Klein, 1984; Nistor

50  and Church, 2005).

Modeling and predicting the entrainment, propagation, and deposition of suspended particles is therefore a challenging task.

Here, we investigate the dynamics of suspended sediment transport in two small watersheds: Capesterre, on the south-east

coast of Basse-Terre Island (Guadeloupe archipelago), and Draix-Laval, in the french Alps. Both catchments are equipped

with gauging stations that record high-frequency measurements of the flow discharge and the turbidity.

55  We begin with a description of Capesterre (section 2). Based on the data collected there, we develop a phenomenological

model of suspended sediment transport, that accounts explicitly for the exchange of small particles between the river bed

and the water column (section 3). We then test the model against the data collected in Capesterre (section 4) and discuss the

physical meaning of its parameters (section 5). Finally, we test the versatility of the model by applying it to the description of suspended-sediment transport in Draix-Laval, a small catchment in the french Alps (section 6).
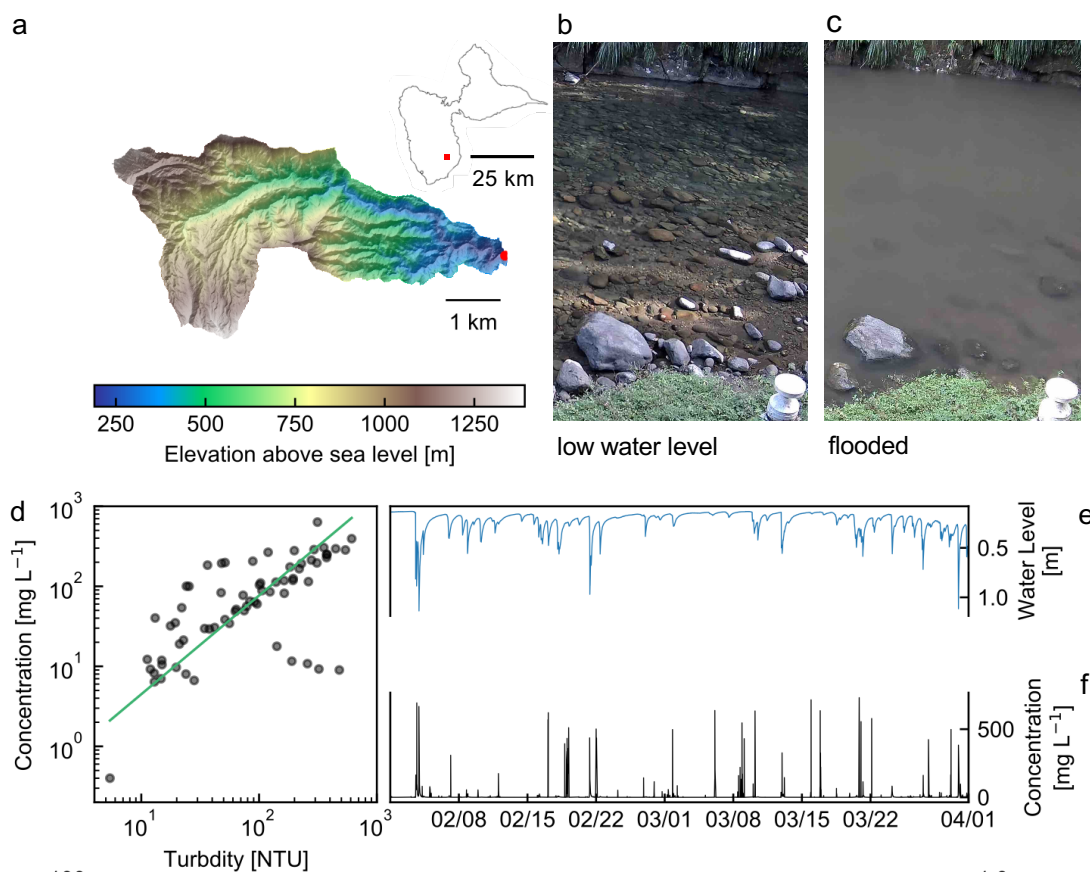
**Figure 1.** Capesterre catchment on Basse-Terre Island, Guadeloupe, French West Indies. (a) Topographic map of the catchment. Inset: map of Guadeloupe (IGN RGE ALTI® 10 m). Red dots locate the catchment outlet on both maps ($16°04'19''$N, $61°36'33''$W). (b) and (c) Images of the river at low and high stage, respectively. (d) Concentration of suspended sediment vs turbidity in the Capesterre river. (e) Water level and (f) concentration of suspended sediment from 02/01/2021 to 04/01/2021.

## 2 The Capesterre catchment

### 2.1 Field site and measurements

We begin our investigation in the Capesterre river, located on Basse-Terre Island. This volcanic island of the Guadeloupe archipelago belongs to the subduction arc of the Lesser Antilles (Feuillet et al., 2002) (Fig.1a). Basse-Terre climate is tropical :

daily temperatures range between 24°C and 28°C, and the annual rainfall rate is about 5200 mm y$^{-1}$. The combination of this

65  tropical climate with a steep volcanic relief produces high erosion rates, that range between 800 and 4000 t km$^{-2}$ y$^{-1}$ (Rad
et al., 2006; Dessert et al., 2015). These values place Basse-Terre Island among the fastest eroding spots on Earth (Summerfield
and Hulton, 1994).

On Basse-Terre, rainfalls are intermittent and occur mainly as short, high-magnitude events. As a result, the discharge of
rivers varies abruptly, with frequent flash floods triggered by tropical rainfalls and hurricanes (Fig.1b and c). These extreme

70  climatic events, particularly frequent during the rainy season from June to January, trigger landslides and debris flows, which
are the main drivers of erosion (Allemand et al., 2014).

The Capesterre river drains a steep watershed, on the windward side of the active Soufrière volcano (Fig 1a). The mean
annual rainfall rate is 5700 mm y$^{-1}$. However, topography induces a strong orographic gradient, and the intensity of rainfalls
is highly heterogeneous within the catchment.

75  Capesterre catchment is underlain by an andesitic bedrock, aged from 400 to 600 ky (Samper et al., 2007). Soils mostly
consist of thin andosols of thickness typically less than 1 m (Colmet-Daage and Bernard, 1979; Lloret et al., 2016). The
Capesterre river flows over 19.7 km, from its headwater on the flanks of the active volcano, at an altitude of 1390 m asl, down
to the Capesterre village, where it discharges into the Atlantic ocean. Its channel is made of bedrock, partly covered by a thin
layer of alluvial sediment. Three kilometers from the sea, the river suddenly turns alluvial, as its slope gradually decreases.

80  The "Observatoire de l'Eau et de l'éRosion aux Antilles" (ObsERA) operates a gaujing station at the site of "La Digue", at an
altitude of 189 m asl, a few hundred meters upstream of the point where the river turns alluvial (Fig.1b and c). At the station, the
river drains a catchment of area 16.4 km$^2$, almost entirely located within the boundaries of the National Park of Guadeloupe.
There, a thick rainforest limits the input of sediment from hillslopes, and anthropogenic forcing is weak.Based on a 4-years
water-sampling campaign, Lloret et al. (2013b) estimated that the mean flux of suspended matter is about $153 \text{t}^{-2} \text{yr}^{-1}$. About

85  10% of this flux consists of Particulate Organic Carbon.

La Digue's station is equipped with a pressure sensor (CS451, Campbell Scientific Inc.) which measures the river stage
relative to the fixed datum defined by a staff gauge installed by the "Direction de l'Environnement, de l'Aménagement et du
Logement" (DEAL-Guadeloupe). In addition, a turbidimeter (OBS3+, Campbell Scientific Inc.) measures the turbidity of the
water. Both pressure and turbidity sensors are connected to a data-logger (Campbell CR800), which records their respective

90  measurements every 5 minutes since 2013 (Fig.1e and f). The station is also equipped with an automatic water sampler (6712
Full-Size Portable Sampler) triggered by a pressure probe (ISCO 720 Submerged Probe module). This device collects water
samples when the river stage exceeds a threshold set by the operator (about 50 cm). Filtration of these samples allows us to
measure the concentration of suspended material $C$ (expressed in $\text{mgL}^{-1}$), and to calibrate the relation between the latter and
the turbidity $T$ (NTU) (Fig.1d). A fit of a power law through our data yields $C = \alpha T^n$, with $\alpha = 0.26$ and $n = 1.23$.

95  The data acquired in the Capesterre river show that the water stage fluctuates, as floods follow each others (Fig.1e). Each
flood starts with an abrupt increase of the water stage – the latter may rise from 0.1 to 1m in less than 1 hour – followed by a
slow recession which last for 12 to 20 hours. In between two floods, the water stage remains low – 10 to 20 centimeters. The

concentration of suspended material, calculated from turbidity, is highly intermittent (Fig.1f) : it is virtually zero 98% of the time, and rises only during floods, where it may reach up to $890 \, \mathrm{mgL}^{-1}$.

## 2.2 Concentration of suspended material

100

Sediment transport in the Capesterre river occurs only during floods. We therefore extract four flood events from our dataset and observe the evolution of the water level and of the concentration of suspended sediment in more details (Fig. 2 and 3). We find that the concentration of suspended sediment follows the fluctuations of the water stage: it is equal to zero before the flood, rises when the water stage exceeds a threshold of about 20 centimeters, increases with the water stage until the flood peak, and

105 finally decreases back to zero during the recession limb of the flood (Fig. 2, left panels).

A closer look at the data, however, reveals a time lag between the flood peak and the concentration peak. For three of the floods we selected, the concentration peak occurs about 30 minutes after the flood peak (Fig. 2, left panels). A plot of the concentration as a function of the water stage better highlights this time lag between concentration and water-level: the concentration vs water-level relation forms an counterclockwise hysteretic loop (Fig. 2, right panels).

110 The flood peak, however, is not systematically ahead of the concentration peak. Sometimes, it is the concentration peak that precedes the flood peak, and the concentration vs water-level relation then forms a clockwise hysteretic loop (Fig. 3).

To determine the proportion of clockwise versus counterclockwise loops in the Capesterre river, we first extract individual flood events from our dataset. To do so, we define a flood as a period during which the water stage is higher than a threshold set to 20 cm. This value roughly corresponds to the threshold above which the flow is strong enough to carry suspended sediment.

115 Based on this definition, we isolate 217 individual floods between May 2019 and December 2021.

We must now determine the direction of the concentration vs water-level relation for each of these floods. Inspired by Langlois et al. (2005) and Misset et al. (2019a), we define, for each flood, the hysteresis index as

$$I_{\mathrm{H}} = \int \widetilde{C} d\widetilde{h}, \tag{1}$$

where we introduce the normalized water level, $\widetilde{h} = (h - h_{\min})/(h - h_{\max})$, and the normalized concentration, $\widetilde{C} = (C - $

120 $C_{\min})/(C - C_{\max})$. $h_{\min}$ and $h_{\max}$ are the minimum and maximum values of the water level $h$ during the flood. Similarly, $C_{\min}$ and $C_{\max}$ are the minimum and maximum values of the concentration $C$ during the flood. With these definitions, both the normalized water-level and the normalized concentration vary between 0 and 1. Accordingly, the hysteresis index $I_{\mathrm{H}}$ ranges between -1 and 1. Negative values correspond to counterclockwise hysteresis, while positive ones indicate clockwise loops.

To characterize the proportion of clockwise versus counterclockwise loops, we just need to compute the hysteresis index

125 $I_{\mathrm{H}}$ for each of the 217 floods of our catalog. We find that this index ranges between -0.719 and 0.452, with a mean value of -0.030, a median of -0.021 and a standard deviation of 0.178. A plot of the cumulative distribution of the hysteresis index reveals that it is negative for 61% of the floods (Fig.4a). In short, 61% of the floods detected on Capesterre are characterized by a counterclockwise loop of the relation between concentration and water-level.

To detect a possible influence of the season, we categorize the flood events by wet (177 events) and dry (44 events) seasons.

130 We then compute the distributions of the hysteresis index for each season, and find that clockwise and counterclockwise

Earth **Surface**
**Dynamics**
Discussions
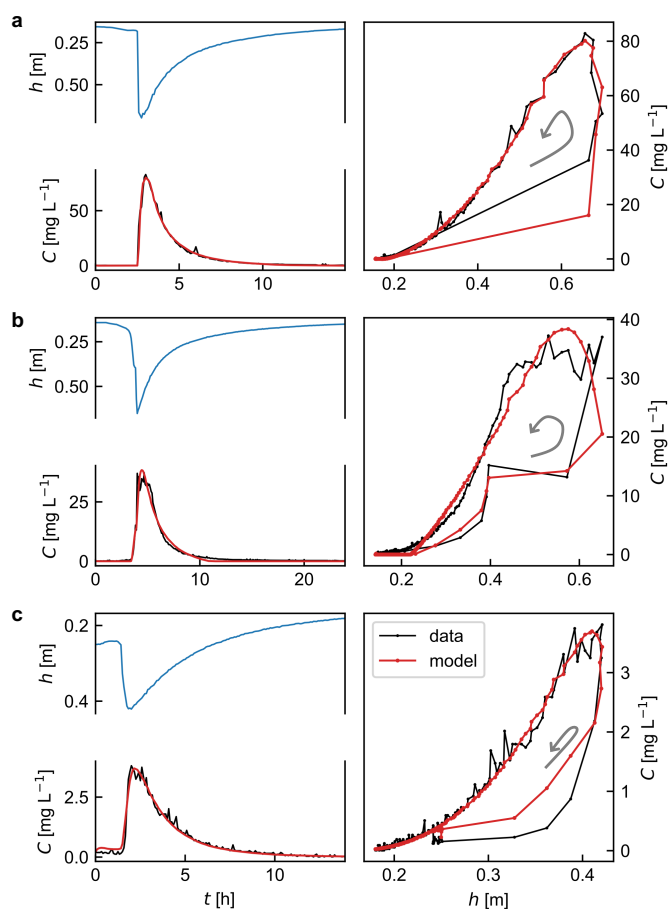
**Figure 2.** Three floods in the Capesterre river for which the concentration vs water-level relation forms a counterclockwise loop. (a) from 09/05/2019 7pm to 09/06/2019 10am, (b) from 07/22/2019 10pm to 07/23/2019 10pm and (c) from 03/11/2021 10am to 03/11/2021 12am. Left panels: time series of the water level (blue line) and the concentration of suspended sediment (black line) measured at the gauging station. Right panels : relation between concentration and water-level. Gray arrows indicate the direction of the hysteresis loops. On each panel, the red line is the concentration predicted from the best-fit model.

hysteresis are equally present in both seasons, with median values very close to zero : -0.007 for the dry season and -0.030 for the wet one (Fig.4b).

To summarize, about 61% of the floods of the Capesterre river exhibit a counterclockwise hysteresis loops, with no influence of the season. In the next section, we therefore focus on counterclockwise hysteretic loops, and try to formulate a simple model, that accounts for their shape.

135
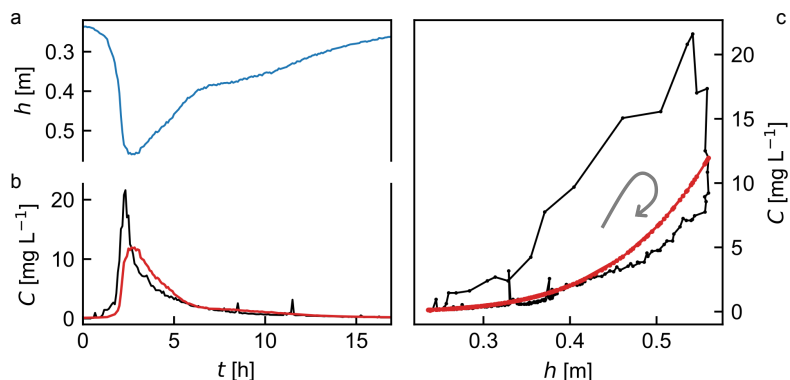
**Figure 3.** Flood recorded in the Capesterre river between 01/15/2021 7am and 01/16/2021 12am. (a) time series of the water level (blue line), and (b) the concentration of suspended sediment (black line) measured at the gauging station. (c) relation between concentration and water-level. Gray arrows indicate the direction of the hysteresis loops. On each panel, the red line is the concentration predicted from the best-fit model.

## 3 Phenomenological modeling of suspended-sediment transport

In this section, we develop a model to account for the evolution of the concentration of suspended sediment in the Capesterre river. Given the complexity of the problem, our objective is not to establish a comprehensive physical theory of suspended sediment transport, but, rather, to derive a phenomenological equation that reproduces our field measurements. We therefore start with a series of simplifying assumptions, driven by field observations.

We first note that the Capesterre catchment is densely vegetated. Accordingly, we assume that, during a flood, the quantity of fine sediment that hillslopes deliver to the river is negligible compared to that originating from the river bed. We shall therefore treat the river bed as the sole source of sediment. We furthermore assume that the quantity of fine sediment stored in the river bed is so large that the entrainment of sediment is not limited by supply, a condition often referred to as "transport limited" (Dietrich et al., 2003). Of course, these two assumptions only hold at the scale of a flood event. Over the longer term, hillslopes processes gradually replenish the river with sediments, compensating for the erosion of the bed during floods. The time scale of this process is uncertain, but it is likely much longer than a few weeks.

Secondly, we observe that the water level in the Capesterre river rarely exceeds 1 meter, a value that remains comparable to the median grain size of its sediment bed, of the order of ten centimeters. Images of the river show that, in these conditions, the turbulence induced by the roughness of the bed is high enough to homogenize the concentration of suspended sediment in the river ( Fig. 1c). Accordingly, we shall neglect any vertical or lateral gradient of the concentration.

Our last and strongest set of assumptions concerns the hydrology of the river. As the size of our catchment is small (about 16 km$^2$), we assume that it responds uniformly to rainfall. In other words, we consider that the water level $h$ rises uniformly along the river, and neglect the propagation of any flood wave. In short, we reduce the complicated problem of the propagation

Earth **Surface**
**Dynamics**
Discussions
EGU
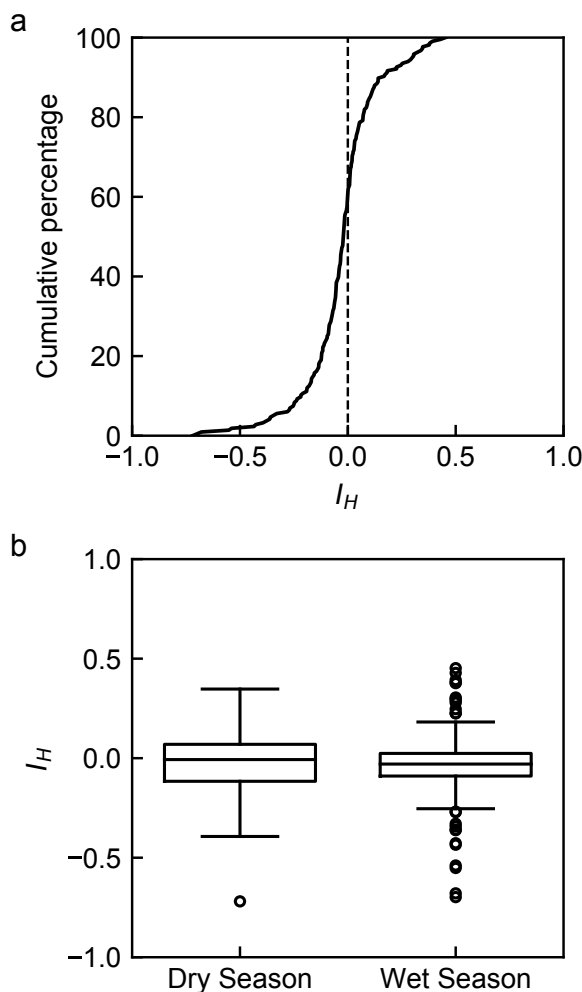
**Figure 4.** (a) Cumulative distribution function (CDF) of the hysteresis index $I_H$ in Capesterre. (b) Distribution of hysteresis indices according to the season.

155 of a concentration wave through a river by neglecting any gradient along its course. The main consequence of this assumption is that it banishes any advection term from the equations, which reduce to a simple ordinary differential equation.

Within the previous set of assumptions, conservation of the mass of suspended sediment reads :

$$\frac{d(hC)}{dt} = E - D \, , \tag{2}$$

where $C$ is the concentration of suspended sediment (mass per unit volume), $h$ is the water-level in the river, and $t$ is time. $E$
160 is the erosion rate, i.e. the mass of sediment entrained from the river bed per unit time and area. Conversely, $D$ denotes the deposition rate, i.e. the mass of sediment deposited on the river bed per unit time and area.

To compute the concentration of suspended sediment, we need to supplement equation (2) with expressions for the erosion and deposition rates. Particles in suspension in the river settle under the action of gravity. In the Capesterre river, the concentration of particles never exceeds $0.9 \, \mathrm{gL}^{-1}$, a value small enough to neglect interactions between particles. In these conditions,

165  particles settle at velocity equal to the settling velocity of a single particle, $V_s$. The deposition thus reads:

$$D = CV_s \,. \tag{3}$$

Field data show that the river drives sediment only when the water level exceed a threshold, $h_t$ (i.e., this is due to the required stress to apply on the sediment). Accordingly, we look for an expression for the erosion rate in the form $E = f(h - h_t)$, where $f$ is some unknown function. For lack of additional constraint, we choose the simplest possible form, and propose that:

170  $$E = \epsilon \left( \frac{h}{h_t} - 1 \right)^n H \left( \frac{h}{h_t} - 1 \right) , \tag{4}$$

where $\epsilon$ is a characteristic erosion rate (mass per unit time and bed area), $n$ is a dimensionless exponent, and $H$ is the Heaviside function.

Combining equations (3) and (4) with the mass balance (2) yields:

$$\frac{d\phi}{dt} = \epsilon \left( \frac{h}{h_t} - 1 \right)^n H \left( \frac{h}{h_t} - 1 \right) - V_s \frac{\phi}{h} , \tag{5}$$

175  where we introduce the mass of suspended sediment per unit of bed area, $\phi = hC$. Equation (5) is an ordinary differential equation. It describes how the concentration of suspended sediment evolves in response to the water level $h(t)$, which acts as a forcing function. To compute the sediment concentration, we use the ode package of the scipy.integrate python library to solve equation (5) numerically over a given time period. This procedure yields the mass of suspended sediment per unit of bed area, $\phi$, from which we deduce the concentration $C = \phi/h$.

180  Our model reduces the dynamics of suspended sediment transport to an exchange of particle between the bed and the river, driven by the water level. As the latter must rise before the river can entrain any sediment, our theory can only produce counterclockwise loops of the concentration vs water-level relation. Finally, we did not establish equation (5) on a rigorous physical ground, but derived it from phenomenological considerations. Equation (5) should thus be considered as an ansatz, whose validity will depend on its ability to represent field data.

185  Equation (5) involves four parameters: the characteristic erosion rate $\epsilon$, the threshold water-level $h_t$, the settling velocity $V_s$, and the exponent $n$. To determine the ability of our model to reproduce field measurements, we must find the values of these four parameters that best fit the data. In this aim, we use an optimization procedure described in the next section.

## 4 Application of the model to the Capesterre river

### 4.1 Optimization procedure

190  To test the model against field data, we select a time period, and extract the corresponding data. The latter form a collection of $N$ discrete values of concentration, $C_i^d$, and water level $h_i^d$, measured at times $t_i$, with $i = 1, .., N$. We then solve numerically

equation (5), using the water-level data, $h_i^d$, as the forcing function. The resulting numerical solution depends on the values of the four parameters $\epsilon$, $h_t$, $V_s$, and $n$. To compare it to the field data, we compute the theoretical concentration, $C_i^m$, for each of the $N$ discrete times $t_i$, and estimate the distance between the model and the data from the chi-square function,

$$195 \quad \chi^2 = \frac{1}{N - n_p} \sum_i (C_i^d - C_i^m)^2 \tag{6}$$

where $n_p = 4$ is the number of parameters in our model.

To achieve the best fit between the model and the data, we need to determine the values of the parameters that minimize the chi-square function. For this purpose, we use the Trust Region Reflective algorithm method, implemented in the scipy.optimize.curve_fit function, and used in the model fitting wrapper of LMFIT (Non-Linear Least-Squares Minimization And Curve Fitting for Python) python library (Newville et al., 2016).

This optimization procedure is sensitive to the duration of the time period over which we apply it. In the next section, we discuss the assimilation of field data to our model over short periods of time, corresponding to a single flood event. The case of longer time periods, which encompass several floods events, will be discussed in section 4.3.

## 4.2 Assimilation over a single flood event

Our model can only produce counterclockwise loops of the concentration vs water-level relation. We therefore test it first on the three floods of figure 2, which exhibit such loops. To do so, we set the initial values of the parameters to $\epsilon = 3\,\mathrm{mg\,m^{-2}\,s^{-1}}$ for the entrainment rate, $V_s = 0.001\,\mathrm{m\,s^{-1}}$ for the settling velocity, $h_t = 15\mathrm{cm}$ for the threshold water-level, and $n = 1$ for the exponent of the erosion law. We then apply the optimization procedure described in the previous section, and determine the parameters that best fit the data (Table 1). Despite its simplicity, the model reproduces surprisingly well the evolution of the concentration of suspended sediment measured in the field (Fig. 2).

A plot of the theoretical concentration as a function of the water-level reveals that the model also accounts reasonably well for the hysteretic loop of the concentration vs water-level relation (Fig. 2, right). For the three flood events that we analyze, we find that he model better represents the recession than the rise of the concentration. This may result from a biais of the optimization procedure which favors the recession limb, as the latter contains a greater number of data points than the flood rise.

The best fit parameters vary from one flood to the other (Table 1). The threshold water-level thus ranges from $h_t = 15$ to 23 cm, in agreement with the estimate based on a direct visualization of the data (Fig. 2). The settling velocity $V_s$ varies between $V_s = 6.2\ 10^{-4}$ and $1.39\ 10^{-3}$ m s$^{-1}$. As discussed later, these values are compatible with the settling velocity of quartz grains of size between 10 and 100 $\mu m$. The entrainment rate $\epsilon$ ranges between 0.641 and 21.1 mg m$^{-2}$ s$^{-1}$. We are not aware of any direct measurement of the rate of entrainment of fine particles from a sediment bed, and cannot therefore assess whether these values ares realistic or not. Finally, the exponent $n$ varies between 1.1 and 2.3.

Out of curiosity, we also tested our model against the flood of figure 3, for which the concentration vs water-level relation forms a clockwise hysteresis. As expected, the model completely fails to account for this flood : it underestimates the concentration peak by about 45% and the concentration vs water-level relation is a mere line, instead of an hysteresis.

| Fig. | Catchment | Start time | End time | $I_H$ | $\epsilon$ [mg m$^{-2}$s$^{-1}$] | $h_t$ [cm] | $n$ | $V_s$ [m s$^{-1}$] |
|------|-----------|------------|----------|-------|------|------|------|------|
| 2a | Capesterre | 09/05/19 7pm | 09/06/19 10am | - 0.194 | $21.1 \pm 0.1$ | $17.3 \pm 0.1$ | $1.580 \pm 0.008$ | $1.385 \pm 0.006 \ 10^{-3}$ |
| 2b | Capesterre | 07/22/19 10pm | 07/23/19 10pm | - 0.236 | $16.12 \pm 0.08$ | $22.5 \pm 0.1$ | $1.122 \pm 0.005$ | $7.54 \pm 0.08 \ 10^{-4}$ |
| 2c | Capesterre | 03/10/21 10am | 03/11/21 12am | - 0.278 | $0.641 \pm 0.001$ | $15.02 \pm 0.03$ | $2.300 \pm 0.003$ | $6.22 \pm 0.01 \ 10^{-4}$ |
| 3 | Capesterre | 01/15/21 7am | 01/16/21 12am | + 0.312 | $10^{-12}$ | $0.34 \pm 0.03$ | $5.23 \pm 0.08$ | $0.26 \pm 0.02$ |
| 4 | Capesterre | 02/06/21 6pm | 02/10/21 11pm | - 0.168 | $23.2 \pm 0.09$ | $20.0 \pm 0.1$ | $2.031 \pm 0.007$ | $9.71 \pm 0.06 \ 10^{-3}$ |
| 7a | Draix-Laval | 05/29/16 6am | 05/29/16 11am | - 0.044 | $40.6 \pm 0.1$ | $7.22 \pm 0.03$ | $0.876 \pm 0.004$ | $3.12 \pm 0.01 \ 10^{-3}$ |
| 7b | Draix-Laval | 05/29/16 3pm | 05/29/16 8pm | - 0.249 | $15.3 \pm 0.1$ | $10.5 \pm 0.01$ | $0.500 \pm 0.004$ | $5.08 \pm 0.07 \ 10^{-4}$ |

**Table 1.** Values of the best-fit parameters, $\epsilon, h_t, n, V_s$, and hysteresis index $I_H$ for each time series.

To summarize, equation (5) correctly models the transport of suspended sediment during floods, provided that the latter presents a counterclockwise loop of the relation between concentration and water-level. Yet, the best-fit parameter values vary from one flood to the other. This raises the question of the ability of the model to represent the evolution of the concentration over a long time, with a unique set of parameters. We address this problem in the next section.

### 4.3 Assimilation over a chronicle

To test the ability of equation (5) to represent sediment transport over a time longer than the duration of a single flood, we select a period of 4 days, marked by the occurrence of 4 successive floods, all of them characterized by a counterclockwise loop (Fig. 5). We then apply the optimization procedure, and determine the parameters that best fit the data (Table 1). This unique set of parameters reproduces reasonably well the evolution of the concentration during the four successive floods. The agreement is however not perfect : the model, for example, underestimates the amplitude of the second concentration peak by about 30%, and overestimates the amplitude of the last one by 34% (Fig. 5).

To better assess the quality of the fit, we compute the mass of suspended sediment exported from the catchment by integrating the sediment flux over the entire duration of our time series, $M = \int C \ q \ dt$, where $q$ is the flow discharge. Integrating the concentration data, we find a mass of $M = 1.239 \ 10^3$kg. The same calculation, conducted with the model, yields $M = 1.177 \ 10^3$kg, that is about of 5% smaller than the data. The model therefore provides a reasonable estimate of the mass exported out of the catchment.

Despite this encouraging result, we note that the model better predicts the data when its parameters are optimized on a single flood event, rather than on a series of floods. In short, the best-fit parameter values change from one flood to the next. This raises the question of their physical meaning, a topic we discuss in the next section.

## 5 Physical meaning of the model parameters

The transport of suspended sediment depends on the properties of the sediment, on the specifics of the flow, and on the configuration of the catchment and the river. In our model, these properties are all lumped into the four parameters of equation
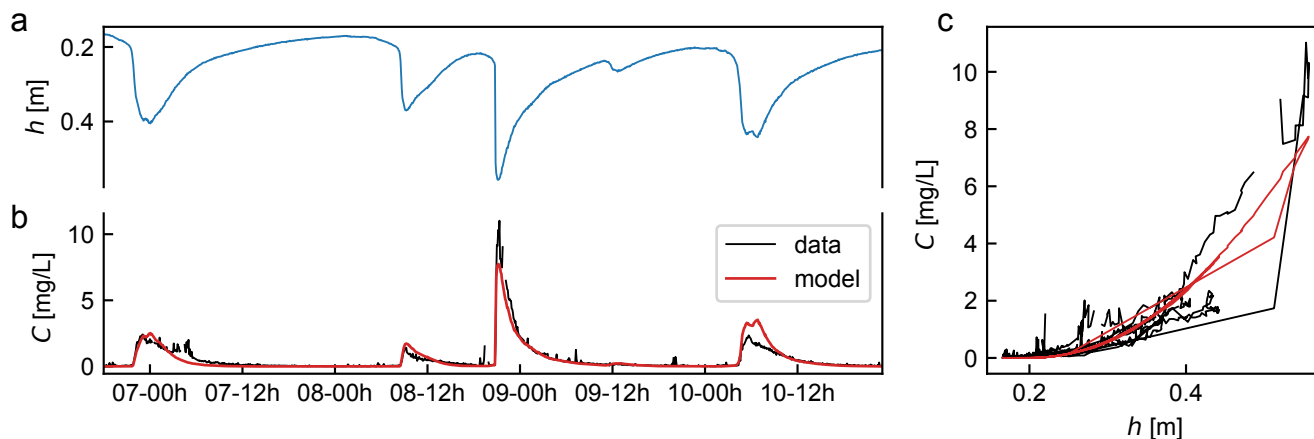
**Figure 5.** (a) Water level (blue line) and (b) concentration of suspended sediment (black line) measured in the Capesterre river over a period of four days, extending from 02/06/2021 6pm to 02/10/2021 11pm. Red line: concentration predicted from the best-fit model. (c) concentration vs water level both observed and predicted.

(5). A change in the value of these parameters from one flood to the next therefore reflects a change of these properties. We suspect, for example, that the characteristic erosion rate $\epsilon$ and the exponent $n$ likely reflect changes in the sediment availability. Explicitly formalizing this relation is, however, a difficult problem. Instead, we now turn our attention to the settling velocity

250 $V_s$ and the threshold water-level $h_t$.

## 5.1 Settling velocity

In our model, the settling velocity $V_s$ is directly related to the rate at which the concentration of suspended sediment relaxes towards zero, after the flood peak. Suspended load usually mobilizes particles with different sizes and, possibly, different chemical compositions and densities. Here, however, we simplify the problem and assimilate the suspended load to a mixture

255 of homogeneous grains.

In the Capesterre river, the concentration of suspended sediment never exceeds $0.9$ g/L, a value small enough to neglect interactions between particles. In this dilute regime, sediments settle at a velocity equal to the settling velocity of a single particle. To compute the latter, we assimilate the suspended sediments to spherical particles of diameter $d_s$ and density $\rho_s$, settling in water of density $\rho = 1000$kg m$^{-3}$ and kinematic viscosity $\nu = 10^{-6}$ m$^2$ s$^{-1}$. The drag force exerted on a particle

260 then reads:

$$F_d = \frac{\pi}{8} C_d \rho d_s^2 V_s^2, \qquad (7)$$

where $C_d$ is a drag coefficient (Andreotti et al., 2013). The latter depends on the settling velocity through the Reynolds number $\mathrm{Re} = V_s d_s/\nu$:

$$C_d = \left[ C_\infty^{1/2} + \left( \frac{24}{\mathrm{Re}} \right)^{1/2} \right]^2 . \tag{8}$$

where $C_\infty$ is a constant that can be set to 1 in the case of natural grains (Andreotti et al., 2013).

Balancing the the drag force with the reduced weight of the particle, $F_g = (\pi/6)(\rho_s - \rho)g d_s^3$, we express the settling velocity,

$$V_s = \left[ \left( \sqrt{\frac{4}{3} \frac{(\rho_s - \rho) g d_s}{\rho}} + 6 \frac{\nu}{d_s} \right)^{1/2} - \left( 6 \frac{\nu}{d_s} \right)^{1/2} \right]^2 \tag{9}$$

where $g$ is the acceleration of gravity. Inverting this equation yields the grain size as a function of the settling velocity :

$$d_s = \frac{24 \, \nu}{\left[ \left( \sqrt{32 \frac{(\rho_s - \rho) g \nu}{\rho V_s} + \frac{V_s}{4}} \right)^{1/2} - \left( \frac{V_s}{4} \right)^{1/2} \right]^2} . \tag{10}$$

The assimilation of field data to our model yields the settling velocities reported in Table 1. Setting the density of sediment to $\rho_s = 2700 \ \mathrm{kg \ m^{-3}}$, we use equation (10) to turn these values into grain sizes. We find that the latter falls between 26 and 125 $\mu$m (Tab.1), in agreement with the range of suspended-sediment sizes reported in the literature (Sheldon et al., 1972; Wilcock et al., 2009).

For lack of simultaneous measurement of turbidity, grain size, and water-level in the Capesterre river, we cannot compare the grain size calculated from the model with that measured in the field. In 2011, however, the observatory ObsERA installed a LISST-StreamSide in the river, and kept it running for a few months. The LISST-StreamSide (Laser In-Situ Scattering and Transmissometry, Sequoia Scientific inc. ) is a laser particle sizer which measures the concentration of suspended particles in 32 logarithmically spaced size classes from 2 to 381$\mu$m (Agrawal and Pottsmith, 2000). Assuming that the sediment size has not drastically changed since 2011, we compare the grain sizes measured by the LISST to that obtained from a fit of our model to the three 2019 floods of figure 2. Figure 6 shows the evolution of the grain size distribution during a flood, on October 30th, 2011. We observe two different behaviors, depending on the grain size. Below a diameter of about 10 $\mu$m, concentration does depend on the water level : it remains finite during the whole flood, and never reaches zero. The corresponding particles, which do not settle on the bed, constitute the wash load. Above about 10 $\mu$m, the concentration of particles follows the evolution of the water level: it increases during the flood rise, and relaxes to zero after the flood peak (Fig.6b, c). The corresponding particles correspond to the suspended load. During the flood, their size ranges from 10 $\mu$m to 168 $\mu$m, a range that is perfectly consistent with the values calculated from the model. Despite its lack of sophistication, the latter can thus be used to infer the characteristic size of the suspended sediment. Encouraged by this result, we now turn our attention to the threshold water-level.
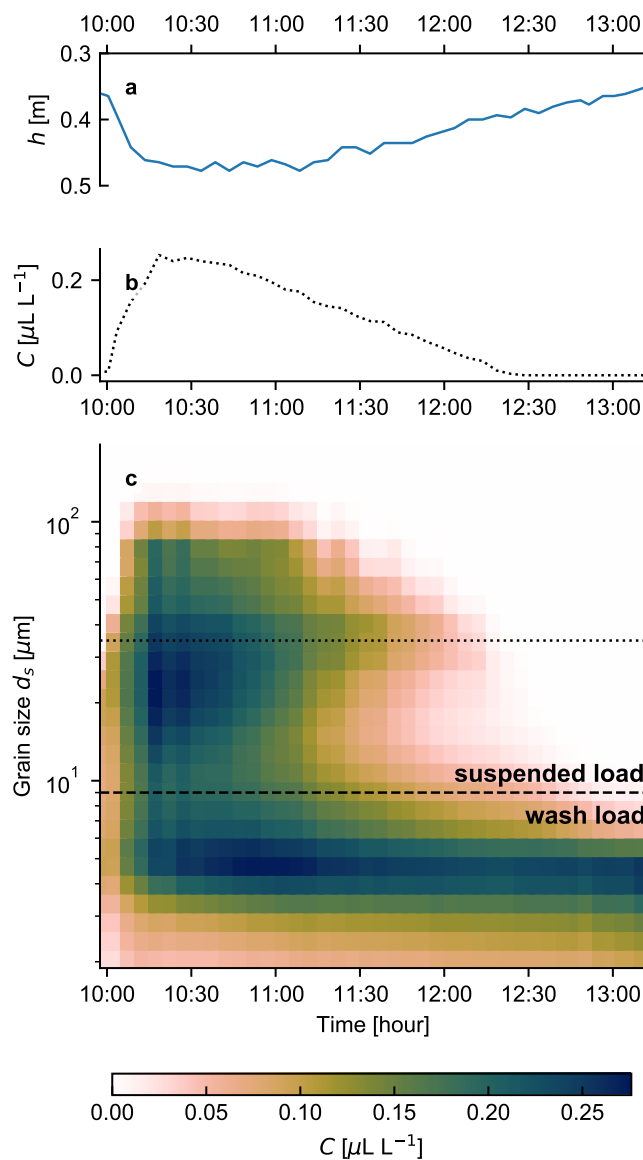
**Figure 6.** Data acquired with a LISST-Streamside in the Capesterre river, on October 30th 2011. (a) water level and (b) concentration of particles of median size 34.8 $\mu$m (class sizes between 31.9 and 37.7 $\mu$m) as a function of time. (c) Evolution of the concentration (color code) as a function of time (horizontal axis) for each of the 32 classes of grain sizes (vertical axis). Dashed line : transition between wash and suspended load. Dotted line : concentration profile displayed in (b).

## 5.2 Threshold water-level

290  In the phenomenological model developed in section 3, the water-level is but a proxy for the shear stress $\tau$ that the river exerts on its bed. For sediment to be entrained by the flow, this stress must exceed a threshold $\tau_t$, a condition usually expressed in terms of the dimensionless Shields stress,

$$\frac{\tau}{(\rho_s - \rho)gd_s} > \theta_t \,, \tag{11}$$

where $\theta_t$ is the threshold Shields stress, a dimensionless number that varies with the grain size and the flow regime (Shields, 295  1936; Andreotti et al., 2013). The fourth parameter of our model, the threshold water-level, should therefore be linked to the threshold Shields stress.

To explicitly relate these two quantities, we invoke the shallow-water theory which approximates the threshold shear-stress by

$$\tau_t = \rho g h_t S \,, \tag{12}$$

300  where $S$ is the slope of the river in the downstream direction. The latter, estimated from a digital elevation model, is about $S = 6.3 \cdot 10^{-2}$ at the La Digue station. Combining equations (11) and (12) yields the threshold water-level as a function of the threshold Shield-stress,

$$h_t = \frac{(\rho_s - \rho)\, d_s\, \theta_t}{\rho\, S} \,. \tag{13}$$

In section 5.1, we found that the size of the suspended particles varies between 26 and 125 $\mu$m. The corresponding threshold 305  Shields stresses range from $\theta_t \approx 0.1$ for the largest grains, to $\theta_t \approx 0.2$ for the smallest ones, which are sensitive to cohesion forces (Shields, 1936; Van Rijn, 1984; Andreotti et al., 2013; Dunne et al., 2022). The corresponding threshold water-level, deduced from equation (13), varies between $h_t \approx 10^{-3}$ and $h_t \approx 10^{-2}$cm. These values are inconsistent with field observations. As the bed of the Capesterre river is covered with centimeter-size sediments (Fig. 1 b), we suspect that this inconsistency might be the signature of bed armoring, an effect commonly observed in gravel bed rivers (Ferdowsi et al., 2017b) as well as on 310  aeolian system (Gao et al., 2016). The river bed is said to be armored when a layer of coarse sediment overlies finer material, preventing it from being entrained in the flow, unless the armoring particles are moved first. If this scenario holds, the threshold of suspended sediment transport should coincide with that of the coarse particles. Measurements of the grain-size distribution of the bed of the Capesterre river, at the La Digue station, indicate that the river bed is predominantly made of gravels and pebbles, with a median grain size $d_{50} \approx 10$cm. The corresponding threshold Shields stress is $\theta_t \approx 3 \cdot 10^{-3}$, for which equation 315  (13) predicts a threshold water-level $h_t \approx 10$cm. This value is consistent with the threshold water-level estimated from the optimization of the model parameters. We therefore conclude that, in the Capesterre river, the threshold of suspended sediment transport is set by that of the coarse particles.

## 6 Versatility of the model

In section 3, we developed a phenomenological model of suspended-sediment transport. Despite its simplicity, this model
accounts for the transport of suspended sediment during floods, provided that the relation between concentration and water-
level forms a counterclockwise loop. We also found that two parameters of the model, the settling velocity and the threshold
water-level, can be used to estimate the size of the suspended sediment and to detect possible armoring of the bed. So far,
however, we have only tested the model on data acquired in the Capesterre River. To test its versatility, we now apply it to the
description of sediment transport in a completely different geological context, that of the Laval catchment.

The Laval catchment, located in the southern part of the French Alps is a small catchment of area $0.86 \text{ km}^2$, drained by
the Laval stream (Fig. 7). Its elevation ranges from 850 to 1250 m a.s.l, and the annual rainfall rate is about $900 \text{ mm yr}^{-1}$,
with heavy rainfall events during spring and summer, and less intense but longer rainfalls in autumn. Besides, this catchment
can also experience snowfalls during winter (Ariagno et al., 2022). Unlike Capesterre, vegetation covers only 32% of the
Laval catchment (Carriere et al., 2020) (Fig.7a). The latter is underlain by easily erodible Middle Jurassic black marls, leading
to the formation of steep badlands slopes within the catchment (Ariagno et al., 2022). A gauging station operated by the
Draix–Bléone Critical Zone Observatory monitors the concentration of suspended sediment and the water level in the stream.
The corresponding data are available on the Draix–Bléone Critical Zone Observatory website.

Figure 7 displays the water level and the concentration of suspended sediment during two floods, extracted from the catalog
of the Draix–Bléone Critical Zone Observatory. The water level ranges from 5 to 25 cm, and the concentration reaches up to
$35 \text{ g L}^{-1}$, that is about 1000 times higher than the maximum concentration measured in Capesterre. During these two floods,
the concentration vs water-level relation forms a counterclockwise hysteretic loop, which makes them, in principle, compatible
with our model (Fig.7b and c, right panels).

Encouraged by this observation, we apply the optimization procedure introduced in section 4.1, and determine the parameters
that best fit the data (Tab. 1). As in Capesterre, we find that the model represents rather well the evolution of the concentration
of suspended sediment measured in the field (Fig.7 b, c). Setting aside the exponent $n$, we note that the best-fit parameter
values fall within the same ranges as those obtained in Capesterre (Tab.1).

A comprehensive evaluation of the model would require a systematic test against data measured not only in Draix Laval, but
in several others catchments. Such a work is beyond the scope of the present paper. For the time being, we simply note that the
model seems able to reproduce sediment transport in a context different than that of Capesterre.

## 7 Conclusions

Based on data acquired in the Capesterre river, a small tropical river in Guadeloupe, we developed a phenomenological model
that accounts for the transport of suspended-sediment. This model reduces the dynamics of suspended sediment transport to an
exchange of particle between the bed and the river, driven by the water level. This simplification has a cost: the model correctly
predicts the transport of suspended sediment during a flood provided that the relationship between concentration and water
level forms a counterclockwise loop. It cannot account, however, for the formation of clockwise loops.
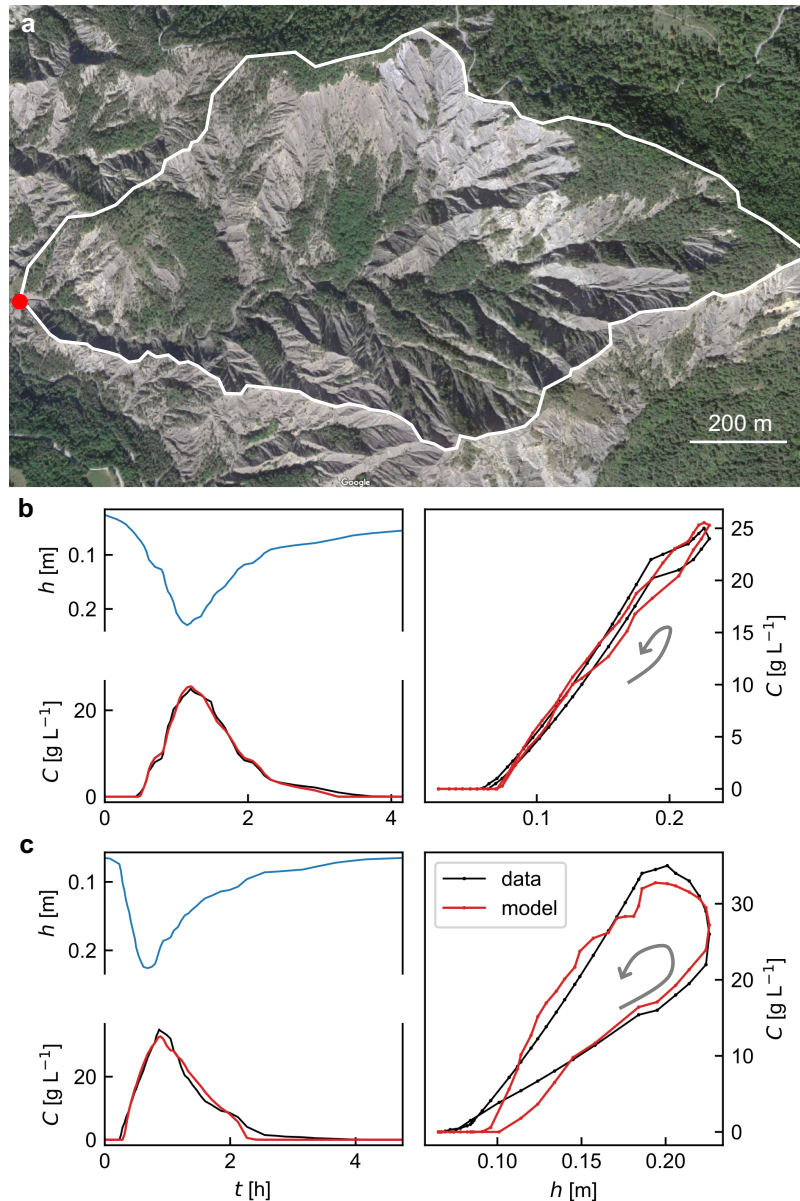
**Figure 7.** Example of floods in the Draix-Laval catchment. (a) Aerial view of the catchment (© Google Maps), red dot locates the outlet where the Laval station is (44°08'26.7"N 6°21'39.4"E). (b) and (c) two floods recorded on 06/29/2016, from 6am to 11am, and from 3pm to 8pm, respectively. Left panels: time series of the water level (blue line) and the concentration of suspended sediment (black line) measured at the gauging station. Right panels : relation between concentration and water-level. Gray arrows indicate the direction of the hysteresis loops. On each panel, the red line is the concentration predicted from the best-fit model (best fit parameters are indicated on the left panel).

Earth **Surface**
**Dynamics**
Discussions

In our model, the characteristics of the sediment and of the river – such as the grain size distribution, the availability of sediment, or the threshold shear stress necessary to set sediment in motion – are all lumped into four parameters. The assimilation of field data to our model shows that these parameters change from one flood event to the next, probably reflecting a change of the properties of the river and of the sediment. The settling velocity $V_s$, and the threshold water-level $h_t$, can be

355 used to estimate the size of the suspended sediment and to detect possible bed armoring. Although we do not demonstrate it, we suspect that the characteristic erosion rate $\epsilon$ and the exponent $n$ are linked to the availability of the sediment.

A test of the model against two floods in Draix-Laval, a small catchment in the french Alps, suggests that the model is versatile enough to be used in diverse hydrological settings, although a comprehensive evaluation of the model would require systematic tests in a larger number of catchments.

360 The model proposed here is far too simple to account for all the mechanisms that influence suspended-sediment transport. It is, for example, unable to produce a clockwise loops of the concentration vs water-level relationship. We believe that this difficulty could be overcome by adding a second equation to the model, that accounts for the amount of fine sediment stored in the bed. Such an improvement is a work in progress.

Finally, our model assimilates the suspended load to a suspension of homogeneous grains. Yet, recent measurements suggest

365 that the chemical composition and the size of the particles suspended in the Capesterre river vary over the course of a flood (C. Dessert, *private communication*). At the beginning of the flood, the suspended load is dominated by litter debris and Allophanes. Sand particles appear later, when the flow discharge is sufficiently high. Modelling such complex behaviour is a difficult problem, which is beyond the capabilities of the model presented in this publication.

*Author contributions.* A.R-B. drove the science, wrote the model and produce the figures. A.L. and E.L. initiated the research. E.L. provided

370 the original concept of the model. A.L. provide his expertise in inverse problem and modeling. E.G. provided the background on erosion in tropical environment. P.A. and C.D. provided data and expertise that support this research. All authors contributed to the paper writing and sharing ideas.

*Competing interests.* Authors declare no competing interests

*Acknowledgements.* All the data used in this paper were collected by the Observatoire de l'Eau et de l'éRosion aux Antilles (ObsERA,

375 INSU-CNRS, http://webobsera.ipgp.fr/) and the Draix–Bléone Critical Zone Observatory (https://bdoh.irstea.fr/DRAIX/), two observatories of the OZCAR research infrastructure. We thank T. Kitou, V. Robert, J. Ajax and B. Lamaille for their technical support. We are also grateful to C. Le Bouteiller for sharing her knowledge and expertise on the Laval catchment. A.L. acknowledge the support from LabEx UnivEarthS (ANR-10-LABX-0023 and ANR-18-IDEX-0001).

# References

380 Agrawal, Y. C. and Pottsmith, H. C.: Instruments for particle size and settling velocity observations in sediment transport, Marine Geology, 168, 89–114, 2000.

Ahn, K.-H. and Steinschneider, S.: Time-varying suspended sediment-discharge rating curves to estimate climate impacts on fluvial sediment transport, Hydrological Processes, 32, 102–117, 2018.

Allemand, P., Delacourt, C., Lajeunesse, E., Devauchelle, O., and Beauducel, F.: Erosive effects of the storm Helena (1963) on Basse Terre

385 Island (Guadeloupe - Lesser Antilles Arc), Geomorphology, 206, 79–86, https://doi.org/10.1016/j.geomorph.2013.09.020, 2014.

Andreotti, B., Forterre, Y., and Pouliquen, O.: Granular media: between fluid and solid, Cambridge University Press, 2013.

Ariagno, C., Le Bouteiller, C., van der Beek, P., and Klotz, S.: Sediment export in marly badland catchments modulated by frost-cracking intensity, Draix–Bléone Critical Zone Observatory, SE France, Earth Surface Dynamics, 10, 81–96, 2022.

Asselman, N. E.: Suspended sediment dynamics in a large drainage basin: the River Rhine, Hydrological processes, 13, 1437–1450, 1999.

390 Bača, P.: Hysteresis effect in suspended sediment concentration in the Rybárik basin, Slovakia, Hydrological Sciences Journal, 53, 224–235, https://doi.org/10.1623/hysj.53.1.224, 2008.

Bagnold, R.: The nature of saltation and of Bedload transport in water, Proc. R. Soc. Lond., A 332, 473–504, 1973.

Battin, T. J., Kaplan, L. A., Findlay, S., Hopkinson, C. S., Marti, E., Packman, A. I., Newbold, J. D., and Sabater, F.: Biophysical controls on organic carbon fluxes in fluvial networks, Nature geoscience, 1, 95–100, 2008.

395 Bierman, P. R. and Montgomery, D. R.: Key concepts in geomorphology, W. H. Freeman and Company Publishers, A Macmillan Higher Education Company, 2014.

Carriere, A., Le Bouteiller, C., Tucker, G. E., Klotz, S., and Naaim, M.: Impact of vegetation on erosion: Insights from the calibration and test of a landscape evolution model in alpine badland catchments, Earth Surface Processes and Landforms, 45, 1085–1099, 2020.

Claudin, P., Charru, F., and Andreotti, B.: Transport relaxation time and length scales in turbulent suspensions, Journal of Fluid Mechanics,

400 671, 491–506, https://doi.org/10.1017/S0022112010005823, 2011.

Colmet-Daage, F. and Bernard, Z.: Contribution à l'Atlas des départements d'Outre-mer: Guadeloupe, Carte des sols de la Guadeloupe, Grande-Terre, Marie-Galante. Carte des pentes et du modelé de la Guadeloupe, Grande-Terre, Marie-Galante. ORSTOM, Antilles, 1979.

Dessert, C., Lajeunesse, E., Lloret, E., Clergue, C., Crispi, O., Gorge, C., and Quidelleur, X.: Controls on chemical weathering on a mountainous volcanic tropical island: Guadeloupe (French West Indies), Geochimica et Cosmochimica Acta, 171, 216–237, 2015.

405 Dietrich, W. E., Bellugi, D. G., Sklar, L. S., Stock, J. D., Heimsath, A. M., and Roering, J. J.: Geomorphic transport laws for predicting landscape form and dynamics, Geophysical Monograph Series, 135, 103–132, https://doi.org/10.1029/135GM09, 2003.

Dunne, K. B. J., Arratia, P. E., and Jerolmack, D. J.: A New Method for In Situ Measurement of the Erosion Threshold of River Channels, Water Resources Research, 58, e2022WR032 407, https://doi.org/https://doi.org/10.1029/2022WR032407, 2022.

D'Avignon, G., Gregory-Eaves, I., and Ricciardi, A.: Microplastics in lakes and rivers: an issue of emerging significance to limnology,

410 Environmental Reviews, 30, 228–244, https://doi.org/10.1139/er-2021-0048, 2022.

Eder, A., Strauss, P., Krueger, T., and Quinton, J. N.: Comparative calculation of suspended sediment loads with respect to hysteresis effects (in the Petzenkirchen catchment, Austria), Journal of Hydrology, 389, 168–176, https://doi.org/10.1016/j.jhydrol.2010.05.043, 2010.

Esteves, M., Legout, C., Navratil, O., and Evrard, O.: Medium term high frequency observation of discharges and suspended sediment in a Mediterranean mountainous catchment, Journal of Hydrology, 568, 562–574, 2019.

415  Ferdowsi, B., Ortiz, C. P., Houssais, M., and Jerolmack, D. J.: River-bed armouring as a granular segregation phenomenon, Nature communications, 8, 1–10, 2017a.

Ferdowsi, B., Ortiz, C. P., Houssais, M., and Jerolmack, D. J.: River-bed armouring as a granular segregation phenomenon, Nature Communications, 8, 1363, https://doi.org/10.1038/s41467-017-01681-3, 2017b.

Feuillet, N., Manighetti, I., Tapponnier, P., and Jacques, E.: Arc parallel extension and localization of volcanic complexes in Guadeloupe,
420    Lesser Antilles, Journal of Geophysical Research: Solid Earth, 107, ETG–3, 2002.

Frey, P. and Church, M.: How river beds move, Science, 325, 1509–1510, 2009.

Gao, X., Narteau, C., and Rozier, O.: Controls on and effects of armoring and vertical sorting in aeolian dune fields: A numerical simulation study, Geophysical Research Letters, 43, 2614–2622, 2016.

Guillon, H., Mugnier, J.-L., and Buoncristiani, J.-F.: Proglacial sediment dynamics from daily to seasonal scales in a glaciated Alpine
425    catchment (Bossons glacier, Mont Blanc massif, France), Earth Surface Processes and Landforms, 43, 1478–1495, 2018.

Hovius, N., Stark, C. P., Hao-Tsu, C., and Jiun-Chuan, L.: Supply and removal of sediment in a landslide-dominated mountain belt: Central Range, Taiwan, The Journal of Geology, 108, 73–89, 2000.

Klein, M.: Anti clockwise hysteresis in suspended sediment concentration during individual storms: Holbeck Catchment; Yorkshire, England, Catena, 11, 251–257, 1984.

430  Koiter, A. J., Lobb, D. A., Owens, P. N., Petticrew, E. L., Tiessen, K. H., and Li, S.: Investigating the role of connectivity and scale in assessing the sources of sediment in an agricultural watershed in the Canadian prairies using sediment source fingerprinting, Journal of Soils and Sediments, 13, 1676–1691, 2013.

Langlois, J. L., Johnson, D. W., and Mehuys, G. R.: Suspended sediment dynamics associated with snowmelt runoff in a small mountain stream of Lake Tahoe (Nevada), Hydrological Processes, https://doi.org/10.1002/hyp.5844, 2005.

435  Liu, Y., Métivier, F., Gaillardet, J., Ye, B., Meunier, P., Narteau, C., Lajeunesse, E., Han, T., and Malverti, L.: Erosion rates deduced from Seasonal mass balance along an active braided river in Tian Shan, Solid Earth Discussions, 3, 541–589, 2011.

Lloret, E., Dessert, C., Pastor, L., Lajeunesse, E., Crispi, O., Gaillardet, J., and Benedetti, M.: Dynamic of particulate and dissolved organic carbon in small volcanic mountainous tropical watersheds, Chemical Geology, 351, 229–244, 2013a.

Lloret, E., Dessert, C., Pastor, L., Lajeunesse, E., Crispi, O., Gaillardet, J., and Benedetti, M. F.: Dynamic of particu-
440    late and dissolved organic carbon in small volcanic mountainous tropical watersheds, Chemical Geology, 351, 229–244, https://doi.org/10.1016/j.chemgeo.2013.05.023, 2013b.

Lloret, E., Dessert, C., Buss, H. L., Chaduteau, C., Huon, S., Alberic, P., and Benedetti, M. F.: Sources of dissolved organic carbon in small volcanic mountainous tropical rivers, examples from Guadeloupe (French West Indies), Geoderma, 282, 129–138, 2016.

Minella, J. P., Merten, G. H., Reichert, J. M., and Clarke, R. T.: Estimating suspended sediment concentrations from turbidity measurements
445    and the calibration problem, Hydrological Processes: An International Journal, 22, 1819–1830, 2008.

Misset, C., Recking, A., Legout, C., Poirel, A., Cazilhac, M., Esteves, M., and Bertrand, M.: An attempt to link suspended load hysteresis patterns and sediment sources configuration in alpine catchments, Journal of Hydrology, 576, 72–84, 2019a.

Misset, C., Recking, A., Navratil, O., Legout, C., Poirel, A., Cazilhac, M., Briguet, V., and Esteves, M.: Quantifying bed-related suspended load in gravel bed rivers through an analysis of the bedload-suspended load relationship, Earth Surface Processes and Landforms, 44,
450    1722–1733, 2019b.

Newville, M., Stensitzki, T., Allen, D. B., Rawlik, M., Ingargiola, A., and Nelson, A.: LMFIT: Non-linear least-square minimization and curve-fitting for Python, Astrophysics Source Code Library, pp. ascl–1606, 2016.

Nistor, C. J. and Church, M.: Suspended sediment transport regime in a debris-flow gully on Vancouver Island, British Columbia, Hydrological Processes: An International Journal, 19, 861–885, 2005.

455 Orwin, J. F. and Smart, C.: Short-term spatial and temporal patterns of suspended sediment transfer in proglacial channels, Small River Glacier, Canada, Hydrological Processes, 18, 1521–1542, 2004.

Park, J. and Hunt, J. R.: Coupling fine particle and bedload transport in gravel-bedded streams, Journal of Hydrology, 552, 532–543, 2017.

Phillips, C. B., Dallmann, J. D., Jerolmack, D. J., and Packman, A. I.: Fine-Particle Deposition, Retention, and Resuspension Within a Sand-Bedded Stream Are Determined by Streambed Morphodynamics, Water Resources Research, 55, 10 303–10 318, 2019.

460 Rad, S., Louvat, P., Gorge, C., Gaillardet, J., and Allègre, C. J.: River dissolved and solid loads in the Lesser Antilles: new insight into basalt weathering processes, Journal of Geochemical Exploration, 88, 308–312, 2006.

Samper, A., Quidelleur, X., Lahitte, P., and Mollex, D.: Timing of effusive volcanism and collapse events within an oceanic arc island: Basse-Terre, Guadeloupe archipelago (Lesser Antilles Arc), Earth and Planetary Science Letters, 258, 175–191, 2007.

Sheldon, R., Prakash, A., and Sutcliffe Jr, W.: The size distribution of particles in the ocean, Limnology and oceanography, 17, 327–340, 465 1972.

Shields, A.: Application of similarity principles and turbulence research to bed-load movement, Ph.D. thesis, Technical University Berlin, 1936.

Smith, H. G. and Dragovich, D.: Interpreting sediment delivery processes using suspended sediment-discharge hysteresis patterns from nested upland catchments, south-eastern Australia, Hydrological Processes: An International Journal, 23, 2415–2426, 2009.

470 Summerfield, M. and Hulton, N.: Natural controls of fluvial denudation rates in major world drainage basins, Journal of Geophysical Research: Solid Earth, 99, 13 871–13 883, 1994.

Suttle, K. B., Power, M. E., Levine, J. M., and McNeely, C.: How fine sediment in riverbeds impairs growth and survival of juvenile salmonids, Ecological applications, 14, 969–974, 2004.

Syvitski, J. P., Peckham, S. D., Hilberman, R., and Mulder, T.: Predicting the terrestrial flux of sediment to the global ocean: a planetary 475 perspective, Sedimentary Geology, 162, 5–24, 2003.

Turowski, J. M., Rickenmann, D., and Dadson, S. J.: The partitioning of the total sediment load of a river into suspended load and bedload: a review of empirical data, Sedimentology, 57, 1126–1146, 2010.

Van Rijn, L. C.: Sediment Transport, Part II: Suspended Load Transport, Journal of Hydraulic Engineering, 110, 1613–1641, https://doi.org/10.1061/(ASCE)0733-9429(1984)110:11(1613), 1984.

480 Wilcock, P., Pitlick, J., and Cui, Y.: Sediment transport primer: estimating bed-material transport in gravel-bed rivers, Gen. Tech. Rep. RMRS-GTR-226. Fort Collins, CO: US Department of Agriculture, Forest Service, Rocky Mountain Research Station. 78 p., 226, 2009.

Williams, G. P.: Sediment concentration versus water discharge during single hydrologic events in rivers, Journal of Hydrology, 111, 89–106, https://doi.org/10.1016/0022-1694(89)90254-0, 1989.

Ziegler, A. D., Benner, S. G., Tantasirin, C., Wood, S. H., Sutherland, R. A., Sidle, R. C., Jachowski, N., Nullet, M. A., Xi, L. X., Snidvongs, 485 A., Giambelluca, T. W., and Fox, J. M.: Turbidity-based sediment monitoring in northern Thailand: Hysteresis, variability, and uncertainty, Journal of Hydrology, 519, 2020–2039, https://doi.org/10.1016/j.jhydrol.2014.09.010, 2014.